The Distribution of Convective and Mesoscale Precipitation in GATE Radar Echo Patterns[1]

CHEE-PONG CHENG AND ROBERT A. HOUZE, JR.

Department of Atmospheric Sciences, University of Washington, Seattle, 98195

(Manuscript received 18 April 1979, in final form 5 July 1979)

ABSTRACT

Quantitative radar data have been used to divide individual radar echoes observed in GATE into convective and mesoscale components. Echoes $<10^2$ km^2 in area were considered, by virtue of their small time and space scales, to be entirely convective. Larger echoes were composed partly of convective regions, characterized by intense fluctuating echo cores, and partly of horizontally uniform mesoscale regions which were less intense and much more slowly varying in structure than the convective regions. The mesoscale regions were apparently associated with widespread precipitating anvil clouds in GATE cloud clusters. About 40% of the total precipitation in GATE fell in these mesoscale regions. The remaining rainfall fell in the convective regions. Only very small amounts of convective rain fell from echoes <5 km in maximum height. Increasing amounts of convective precipitation were associated with echoes of increasing maximum height, from the very small amounts in echoes ≤5 km to a maximum amount from echoes with maximum tops of ~12 km. A secondary maximum of rain was associated with overshooting echoes reaching 15–16 km. Overshooting was rare in early summer when the level of zero buoyancy was near 11 km, and more common in mid to late summer when the level of zero buoyancy was near 14 km. When the overshooting echoes were accompanied by weak large-scale upward motion they were relatively isolated, whereas when the overshooting coincided with strong large-scale forcing, the echoes were more widespread. Major events of mesoscale anvil rainfall were always associated with convective echoes which had maximum tops reaching the level of zero buoyancy, and they tended to occur when the large-scale upward motion was enhanced.

1. Introduction

A principal objective of the Global Atmospheric Research Program's Atlantic Tropical Experiment (GATE) was to develop a better understanding of the role of the convective clouds that prevail throughout the Intertropical Convergence Zone (ITCZ), of particular interest being the interactions of these clouds with large-scale flow patterns. The importance of this problem was emphasized by Riehl and Malkus (1958), who showed that deep cumulonimbus clouds containing nearly undiluted updrafts (hot towers) constitute the only plausible way in which large-scale heat losses in the tropical upper troposphere can be accounted for. According to their hypothesis, the hot towers carry air of high moist static energy upward from the boundary layer to the upper troposphere. More recent studies of the mass and heat budgets of synoptic-scale disturbances in the ITCZ have shown that the entire spectrum of convective clouds, ranging from small trade cumulus to deep cumulonimbus of the type discussed by Riehl and Malkus, is involved in the large-scale heat balance (Yanai *et al.*, 1973; Ogura and Cho, 1973; Johnson, 1976).

These studies, however, were not based on observations of the clouds themselves. The spectrum of clouds, instead, was diagnosed from observed large-scale mass and heat budgets. Direct observations of convective cloud populations in the tropics have been based on cloud photography for smaller cumulus clouds (Malkus and Riehl, 1964; Plank, 1969) and on radar observations for deeper precipitating clouds (López, 1973, 1976, 1978; Houze and Leary, 1976; Houze and Cheng, 1977). Our present paper falls into the latter category, as it is also concerned with radar observations of cumulonimbus populations. It is a continuation of the work described in our previous paper (Houze and Cheng, 1977) which was a statistical survey of the qualitative characteristics of GATE radar echo patterns. We did not at that time have available sufficient information regarding GATE radar calibrations and intercomparisons to derive quantitative precipitation intensities from the radar data. With this information now available, we have been able to determine the rainfall rates in each of the echoes sampled in our previous studies. Using these rates we have characterized the population of precipitat-

[1] Contribution No. 502, Department of Atmospheric Sciences, University of Washington.

0027-0644/79/101370-12$07.00

ing clouds in GATE by determining the distribution of total rain among echoes of various sizes and types. We refer to this distribution as a precipitation spectrum for GATE.

In his work with radar data, López (1973) characterized a population of tropical cumulonimbus by determining the frequency distribution of radar echo lifetimes. Using a cloud model, he computed the properties of cumulonimbus clouds producing echoes of various lifetimes. Then, combining the model cloud properties with the observed frequency distribution of echo lifetimes, he calculated the net heating by the observed population of clouds. Taking a somewhat different approach, Houze and Leary (1976) characterized a population of tropical cumulonimbus clouds by finding the amount of precipitation associated with radar echoes of different maximum heights (i.e., a precipitation spectrum). A cloud model was used to calculate the convective mass and heat transports, which were necessarily accomplished by the clouds in producing the observed amount of precipitation in each echo height category. The net upward heat flux by the cloud population was obtained by integrating over all of the height categories in the precipitation spectrum.

All previous calculations of large-scale heating by populations of tropical convective clouds, whether diagnosed from large-scale mass and heat budgets or computed from radar observations of the clouds themselves, have assumed that the cloud vertical motions were contained entirely in cumulus-scale updrafts and downdrafts. However, the radar studies of López (1976, 1978) and Houze and Cheng (1977) show that major portions of radar echo populations over tropical oceans are made up of large mesoscale radar echoes $\sim 10^3$–10^4 km^2 in area. While these mesoscale echoes contain intense embedded cumulus-scale ($\sim$1–10 km^2) and small mesoscale ($\sim 10^2$ km^2) cores of very intense rainfall, Houze (1977) and Leary and Houze (1979a,b) have shown that large areas within them also consist of horizontally uniform precipitation, which apparently falls from widespread anvil clouds. In Houze's (1977) tropical squall-line system, the horizontally uniform rain accounted for 40% of the total precipitation.

It has been argued that the precipitation from tropical anvil clouds is associated with mesoscale, as opposed to cumulus-scale, vertical air motions (Zipser, 1969, 1977; Houze, 1977; Leary and Houze, 1979a,b). Brown (1979) has reached the same conclusion with a numerical model which develops a mesoscale updraft above the 700 mb level in the anvil cloud of a tropical squall-line system and a mesoscale downdraft driven by evaporation of rain below the base of the anvil cloud. Sanders and Paine (1975), Sanders and Emanuel (1977) and Ogura and Chen (1977) have found mesoscale circulations associated with the anvil clouds of deep convective systems in midlatitudes. If a substantial portion of tropical precipitation consistently falls from anvil clouds, then the mesoscale vertical circulations associated with the anvils need to be accounted for in assessing the effects of cloud motions on large-scale flow patterns, just as do the cumulus-scale updrafts and downdrafts in convective towers.

We have kept this problem in mind in deriving a precipitation spectrum for GATE. The spectrum first divides the total observed rainfall into its mesoscale and convective components, the mesoscale component being the portion of the total rain which fell from the horizontally uniform regions of large echoes. The convective part of the spectrum is composed of the sum of all of the rain from intense cumulus-scale echo cores, which occurred either as small isolated echo entities or as embedded cores within the large echoes.

From this spectrum, we obtain an indication of the relative importance of mesoscale and convective cloud circulations in GATE. The convective portion of the precipitation spectrum is further subdivided to give the amount of precipitation associated with convective echoes of different maximum heights. This part of the spectrum is similar to that used by Houze and Leary (1976) as input to their calculations of convective mass and heat transports. It indicates the relative importance of convective clouds of various depths.

By characterizing the precipitation in GATE according to whether it was purely convective or occurred in horizontally uniform mesoscale regions, and by further indicating the relative importance of convective cells of different maximum heights, the precipitation spectrum provides insight into the nature of the precipitation-producing clouds in GATE. In the sections below, we examine further how the precipitation spectrum varied over the summer season and how it responded to large-scale stability and upward motion. In a future paper, the GATE precipitation spectrum will be used as input to appropriate cloud models in evaluating the relative importance of convective and mesoscale motions in the large-scale mass and heat budgets over the GATE array.

2. The radar data

The radar data used in this study were obtained with the radar system on board the U.S. NOAA ship *Oceanographer*. This radar system [described in detail by Hudlow (1975)] was one of four quantitative C-band systems used in GATE. It had a wavelength of 5.3 cm, a beamwidth of 1.5° and a peak power of 215 kW. It was used to make three-dimensional scans at 15 min intervals throughout

GATE. A three-dimensional scan consisted of a series of 360° azimuthal sweeps at elevation angle increments of ~2°, ranging from 0.6° to 22°.

The *Oceanographer* radar system processed its returned signals with an analog video integrator processor (AVIP) and a digital video integrator processor (DVIP) operating in parallel. Signals processed by the AVIP were displayed in real time on a Plan Position Indicator (PPI), where they were contoured in intervals of 8 dBZ. The real time AVIP displays on the PPI were photographed in time lapse and the signals processed by the DVIP were recorded on magnetic tape in real time. After the field phase of GATE the DVIP data were further processed to produce low-level horizontal maps of the numerical values of the radar reflectivity averaged over 4 km by 4 km square grid spaces (Hudlow, 1976). To produce nearly horizontal maps of the low-level reflectivity pattern, DVIP data from the first three elevation angles of the three-dimensional scans were composited to generate 130 × 130 Cartesian arrays, in which each element of the array was the equivalent reflectivity (expressed in dBZ) averaged over a particular 4 km × 4 km grid square. The maps extend to a horizontal distance of 260 km from the radar.

A unit of dBZ is defined here according to usual convention, as

$$\mathrm{dBZ} = 10 \log_{10} Z_e, \tag{1}$$

where Z_e is the equivalent reflectivity factor ($\mathrm{mm^6\ m^{-3}}$). The conversion to dBZ from the DVIP data was accomplished through the results of careful calibrations of the *Oceanographer* radar including intercomparisons with the other three GATE quantitative radars (Hudlow *et al.*, 1979). These calibrated horizontal reflectivity patterns are referred to by Hudlow (1976) as *hybrid* echo patterns since three elevation angles were used to construct time. The final reflectivity in each grid square of the hybrid patterns, computed by Hudlow to within 1 dBZ, were recorded on magnetic tape. Maps of the hybrid echo patterns were also printed out by Hudlow on microfilm with 3 dBZ resolution.

The values of reflectivity in the hybrid data were related to R ($\mathrm{mm\ h^{-1}}$) through a Z-R relationship of the standard form

$$Z_e = aR^b, \tag{2}$$

where a and b are constants (Battan, 1973). We used the values $a = 230$ and $b = 1.25$, which were used by Hudlow (1978) and are based on GATE shipboard observations of raindrop size distributions. Reanalysis of the shipboard drop-size measurements has led to the revised values, $a = 180$ and $b = 1.35$ (Austin and Geotis, 1979). The Z-R relationship, which uses these new values of a and b, actually differs very little in practice from the one we used. Nor would our study be significantly affected by using the values $a = 170$ and $b = 1.52$ derived by Cunning and Sax (1977) from GATE airborne drop-size measurements.

The hybrid data did not include corrections for instrumental biases and attentuation resulting from absorption of carbon dioxide and oxygen. We have incorporated Hudlow's (1978) later corrections for these effects into our rainfall rates.

It has been shown by comparison with individual raingages (Hudlow *et al.*, 1979) and in synoptic-scale moisture budget studies (Thompson *et al.*, 1979) that, after all corrections and calibrations are applied to the hybrid data, accurate rainfall maps are obtained.

3. Methods of analysis

When we undertook our first study of GATE radar echo patterns (Houze and Cheng, 1977), only the time-lapse motion pictures of the AVIP displays of the PPI were available. Using these data, we identified all of the echoes appearing on the *Oceanographer's* PPI at 1200 (all times GMT) on each day of GATE that the radar was operative. Each of these echoes was then named and tracked, and the maximum height it reached during its lifetime was determined, but we made no attempt to compute the amount of rain which fell from each echo. In our present study, for each of the echoes named and tracked previously, we used the hybrid data from the *Oceanographer* radar to determine the instantaneous rate at which rain was falling from each echo at 1200 GMT. Before calculating this flux of rain, however, the echo was divided into its *convective* and *mesoscale* regions, which were distinguished in the following way.

Any echo $\leqslant 10^2$ km^2 was considered to be entirely convective. Besides being small, these echoes had short lifespans characteristic of convective-scale phenomena (generally less than 60 min) and they lacked any identifiable substructure.

Larger echoes ($\geqslant 10^2$ km^2 in area) presented a problem because they are too big to be considered convective scale. However, such an echo may be wholly or partially composed of an irregular, rapidly fluctuating pattern of convective elements within the large parent echo. Echoes in the range of 10^2–10^3 km^2 in area appear to consist almost exclusively of aggregates of growing and dissipating convective cells (López, 1978). Larger echoes, especially those ~10^4 km^2 in area, are still more complex as they may consist partly of aggregated convective cells, while being partly, or sometimes almost wholly, covered by rain which is horizontally homogeneous and slowly evolving compared to the fluctuating and more intense convective part of the pattern. This horizontally uniform rain is probably associated with

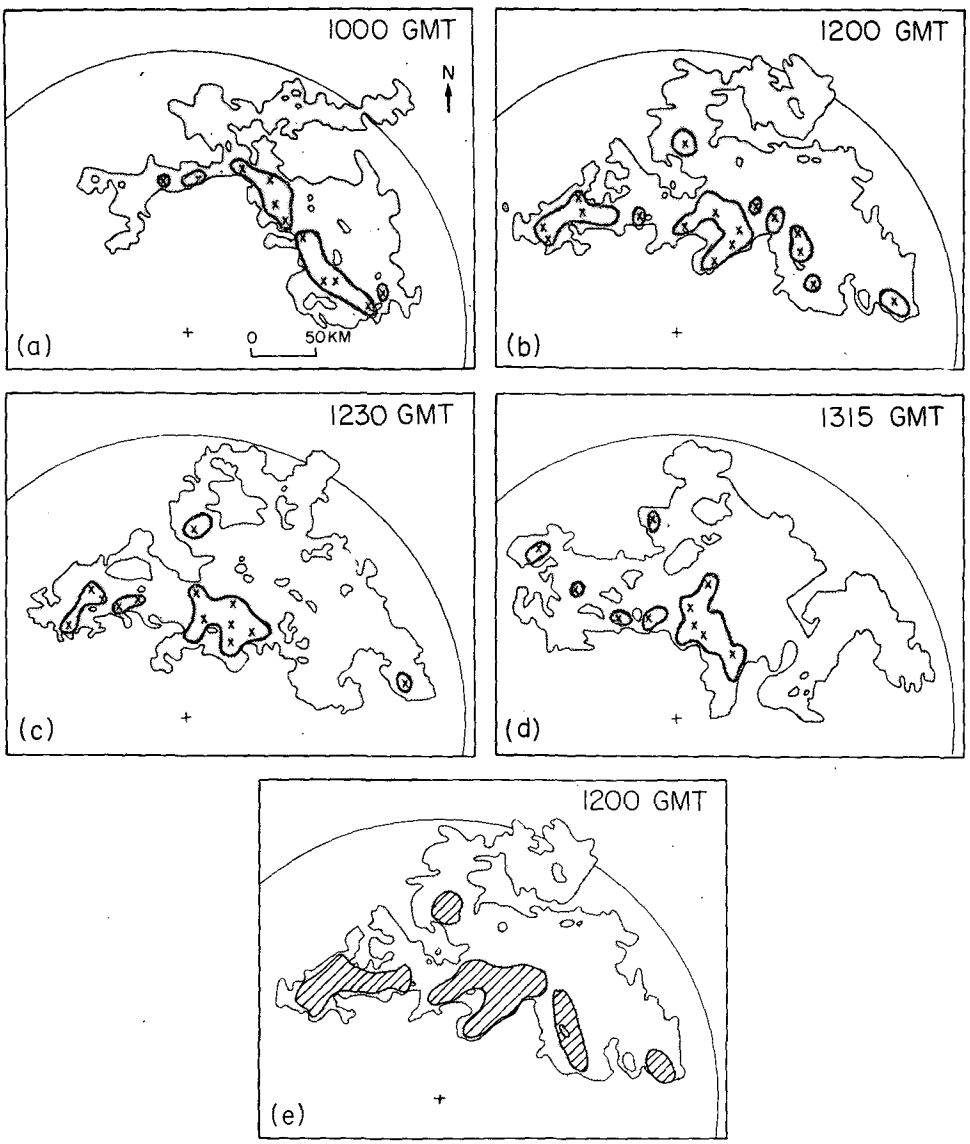

FIG. 1. Illustration of convective and mesoscale regions for echo (shaded) appearing on the *Oceanographer* radar (located at plus mark in lower center of each frame; 7.75°N, 22.2°W) on 5 September 1974. In (a)–(d), active regions (see text for definition) are outlined with a heavy line. Reflectivity peaks are shown by an ×. In (e), the convective regions (see text for definition) are cross-hatched.

anvil clouds (Houze, 1977; Leary and Houze, 1979a, b). Because of its large horizontal extent and longer time-scale, we refer to the horizontally uniform portion of a large echo as its *mesoscale* region since the dynamical and physical processes in that region are evidently larger in scale than those in the irregular, rapidly varying part of the echo, which we call the *convective region*. We used the following specific criteria for distinguishing the convective and mesoscale regions of each large echo seen in the *Oceanographer* echo patterns at 1200 GMT.

The hybrid reflectivity pattern for each large echo was examined at 15 min intervals throughout its lifetime. At each observation time, the *active regions* of the echo were identified as embedded echo regions that stood out from the general background echo. The active regions were identified visually by the analyst, and some subjectivity was involved. The difficulties of applying purely objective methods to identify echo features when their identification depends on several factors of echo structure and development are well known (see, e.g., the comments of López, 1978). We tried to minimize the effects of subjectivity in our visual analysis by employing the following rules.

An initial identification of the active regions

present in a large echo at a given time was made using the general rule that the average rainfall rate in an active region exceeded the general background rate by about a factor of 3 or more. No restriction was placed on the horizontal area covered by an active region, as it might consist of just one echo core or of several contiguous cores. After its initial identification, an active region was subjected to a further examination in time. Although the entire active region might last for up to 3 h or more, to qualify as an active region its internal structure had to exhibit a convective time scale whereby the individual cores of peak reflectivity in the active region underwent lifetimes ≤ 1 h. Thus, the active regions stood out not only as the regions of generally high reflectivity within a large echo, but also as regions composed of a rapidly fluctuating pattern of echo cores in various stages of development.

Examples of the active regions at several times during the lifetime of a large echo which occurred on 5 September 1974 are shown in Figs. 1a–1d. The active regions identified in this echo agree in location with the regions of convective cells identified by Leary and Houze (1979a) in their study of the full three-dimensional structure of this echo. They found that inside the active regions, the echo consisted of vertically oriented intense cores, in various stages of convective growth or dissipation, while outside the active regions the echo was comparatively horizontally homogeneous at all levels (see, for example, Fig. 7 of Leary and Houze, 1979a). They further examined aircraft data obtained in the echo between 1200 and 1300 both inside and outside the active regions. Outside the active regions, aircraft temperature and dew-point measurements suggested the presence of a mesoscale evaporative downdraft of the type found by Zipser (1969, 1977) below precipitating anvil clouds (see Fig. 8 of Leary and Houze, 1979a), while inside an active region of airborne wind measurement showed evidence of convective-scale downdraft activity (Fig. 9 of Leary and Houze, 1979a). These observations give us confidence that our method of identifying the convectively active regions of large echoes is reasonably accurate.

After identifying its *active regions* at 15 min intervals, attention was focused on the large echo as it appeared at 1200 (e.g., Fig. 1e). The *convective region* of the echo at this time was defined as the union of its currently active regions and those regions of the echo which had been part of an active region in the immediate past (≤ 2 h before 1200) or were to become part of an active region in the near future (≤ 2 h after 1200). By this definition, the convective region contained all of the precipitation in the echo at 1200 GMT which was associated with convection that was currently active or was in the process of forming or dissipating. Remnants of convection, which had existed a long time in the past (>2 h) but had completely lost its convective identity and blended into the background rain by 1200 GMT, were not included in the convective region.

The *mesoscale region* of the large echo was defined as all of the echo outside of the convective region at 1200. This region excluded all the highly intense fluctuating portions of the large echo, and tended to be horizontally uniform in intensity and slowly varying in time compared with the convective region. Usually, the convective region occupied most of the area of an echo leaving only a negligible amount of mesoscale rain outside the convective elements. As found by López (1978), almost all echoes from 10^2 to 10^3 km^2 in area fit this description. However, the very largest echoes, those $\sim 10^4$ km^2 in area, typically had quite large mesoscale regions. These mesoscale regions, in fact, considerably exceeded their accompanying convective regions in areal coverage and, although the rain in them was less intense, they covered such large areas that they precipitated, as we shall see, almost as much rainwater as did the more intense, but smaller, convective regions. It is these very large mesoscale regions that appear to be associated with anvil clouds. In detailed case studies (Houze, 1977; Leary and Houze, 1979a,b), the mesoscale anvil rain has been found to be characterized by a prominent radar bright band. When our present criteria are applied to the same cases, the mesoscale rain areas identified coincide with the areas exhibiting bright bands. Detailed analyses for bright bands could not be carried out for all cases considered herein, but we believe that the mesoscale rain areas identified in the present study were generally consistent in structure with those examined in the case studies.

Using the instantaneous rainfall rates derived from the hybrid radar reflectivity patterns, we computed the mass of rainwater falling at 1200 GMT from the mesoscale region (if any) of each named echo in Phases I, II and III of GATE. These values were summed to obtain the percentage contribution of the mesoscale component to the total rain in each phase of GATE. The identified convective regions in each named echo were grouped into categories of the maximum echo height reached during their lifetimes. The method by which the maximum echo heights were defined and determined is discussed by Houze and Cheng (1977). The masses of rainwater that fell from the convective regions in each echo height category were then summed over Phases I, II and III of GATE.

The result of these calculations was a spectrum of rainfall for each phase of GATE showing the percentage of the total rainfall which was mesoscale in character and the percentage which was associated with convective regions of various maximum echo heights.

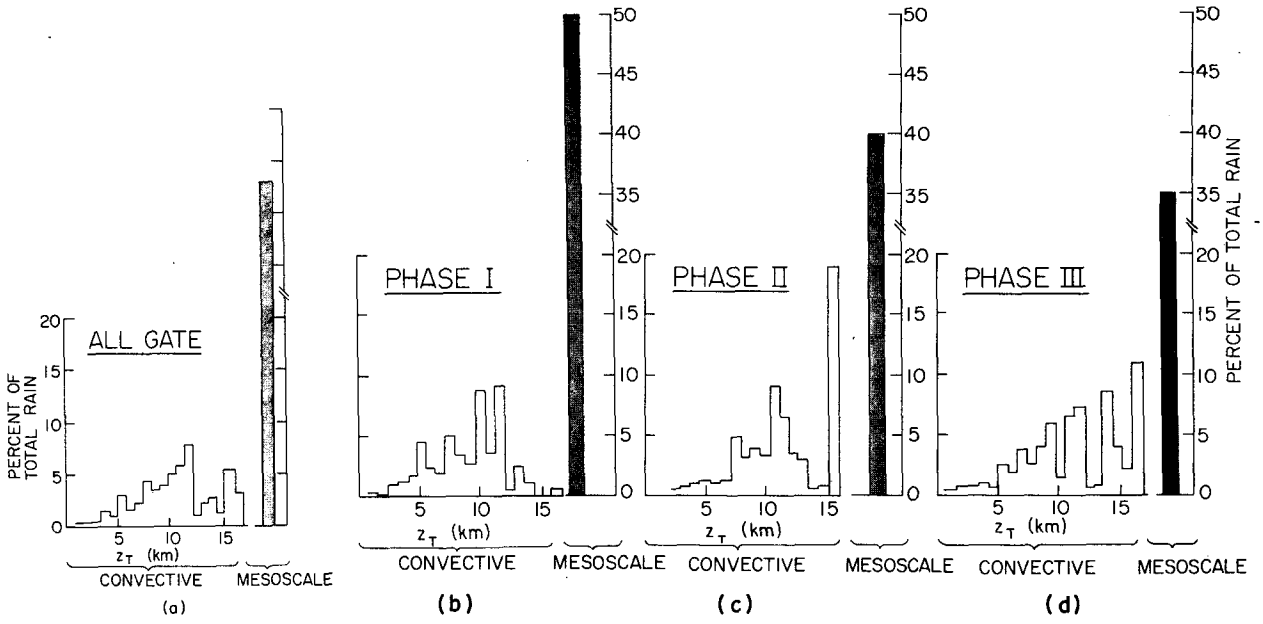

FIG. 2. Precipitation spectra derived from *Oceanographer* radar.

4. The observed precipitation spectrum

The rainfall spectrum derived for all of GATE and for each of the three phases of GATE, corresponding to early, middle and late summer[2], are shown in Fig. 2. From Fig. 2a, it can be seen that a little over 40% of the total rain in GATE was found to be mesoscale by the criteria described above. This result suggests that the mesoscale anvil rain described by Houze (1977) and Leary and Houze (1979a,b) is a general enough phenomenon in the ITCZ to be prominent in average conditions as well as in specific cases.

Comparing Figs. 2b–2d, we see that the amount of mesoscale rain decreased from 50% of the total rain in Phase I to 40% in Phase II and 36% in Phase III. This variation may not be large enough to be significant, but the trend is consistent with the results of our previous study (Houze and Cheng, 1977) in which we found that the intensity of convective precipitation, as indicated by the numbers, heights and peak reflectivities of intense echo cores, increased from Phase I to III of GATE. The decreasing percentage of mesoscale rain over the summer does not, however, reflect a diminution in the amount of mesoscale rain which fell. Rather the mesoscale rain increased *proportionately* less than the convective rain between Phases I and III.

An important question is: how certain are the values of 36 to 50% that we have found for the fraction of total rain that occurs in quasi-uniform mesoscale areas? Because of the arbitrariness of the definitions of convective and mesoscale echoes and the subjectiveness in visually identifying echo features, according to these definitions, there are some uncertainties in our results. We feel, however, that the most significant convective echo regions were so obvious that they would be difficult to overlook by any method and, consequently, the uncertainty in the amounts convective and mesoscale rain probably does not exceed 10–15%. Since our samples were all taken at 1200 GMT, and since diurnal cycles have been noted in GATE (Gray and Jacobson, 1977; McGarry and Reed, 1978), there may also be a slight diurnal bias in our results.

The convective rain is presented in Fig. 2 as a function of the maximum echo height of the convective region with which it was associated. In general, very little precipitation was associated with maximum echo tops <5 km. The all-GATE spectrum (Fig. 2a) shows a steady increase (positive correlation) in the amount of precipitation with increasing maximum echo top from 5 to 12 km, then a sharp drop to a minimum between 12 and 15 km and a second major maximum at 15–16 km. Thus, there appear to be two convective regimes, one in which the clouds penetrate (or overshoot) the tropopause (~14 km) and the much more common one in which they do not.

From Figs. 2a–2d, it can be seen that the amount of rain associated with overshooting echoes was large. However, this result does not mean that an inordinate amount of air in convective updrafts actually penetrated the tropopause region. The maximum height of an individual convective region was usually attained only temporarily during its life-

[2] Phase I was from 28 June–16 July, Phase II from 28 July–15 August, and Phase III from 30 August–17 September 1974.

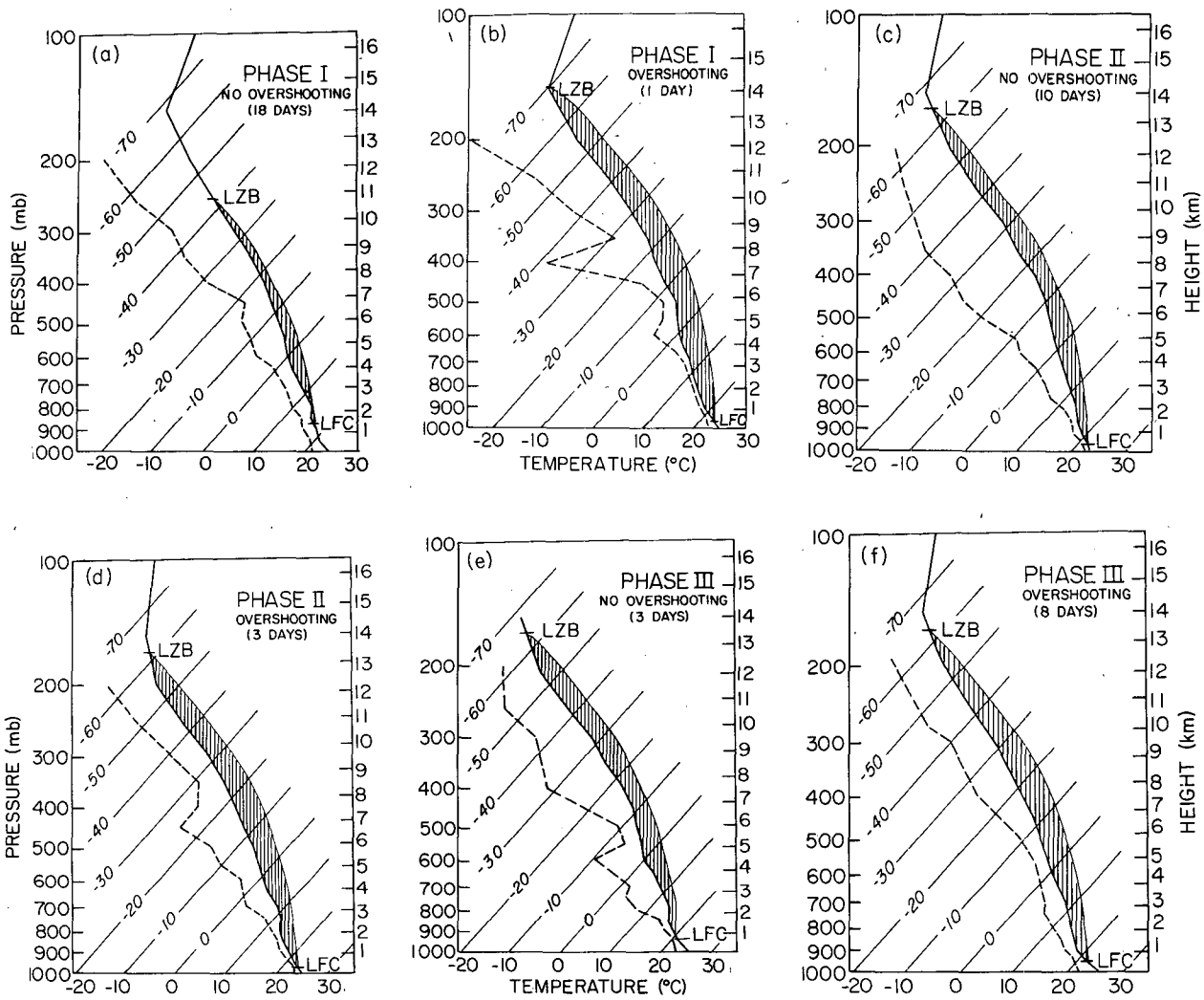

FIG. 3. Mean soundings for *Oceanographer* plotted on a skew T-log$p$ diagram. LFC is the level of free convection, LZB the level of zero buoyancy, and the positive area, defined by the moist adiabat from LFC to LZB, is cross-hatched. Temperature curves are solid, dew point dashed.

time and only by a small portion of the total area covered by the convective region. Thus, most of the mass transport in the updrafts of such a convective region was probably confined below the tropopause with the overshooting occurring only for short time intervals in its most intense spots. The percentage of rain associated with overshooting convective regons increased considerably from Phases I to III (Figs. 2b–2d). This finding is again consistent with the presence of more intense convection later in the summer reported by Houze and Cheng (1977).

5. Large-scale conditions associated with overshooting echoes

The association of significant amounts of precipitation with overshooting echoes raises questions concerning the large-scale conditions which give rise to the overshooting, specifically, whether there is a particular type of static stability or large-scale forcing involved. The static stability on days with and without overshooting is indicated in Fig. 3 by the average of the *Oceanographer* soundings taken within a 6 h period centered on 1200.[3] Overshooting days are considered to be those on which the maximum echo top (reached during the lifetimes of echoes present on the *Oceanographer* radar at 1200) exceeded 14 km. To indicate the effect of large-scale forcing we constructed Fig. 4, which compares the daily values of the maximum echo tops with the time sequence of the average 700 mb vertical veloc-

[3] The *Oceanographer* soundings were taken at 3 h intervals. GATE upper air data are available through the *GATE Data Catalog*, Environmental Data Service, Federal Bldg., Asheville, N.C. 28801.

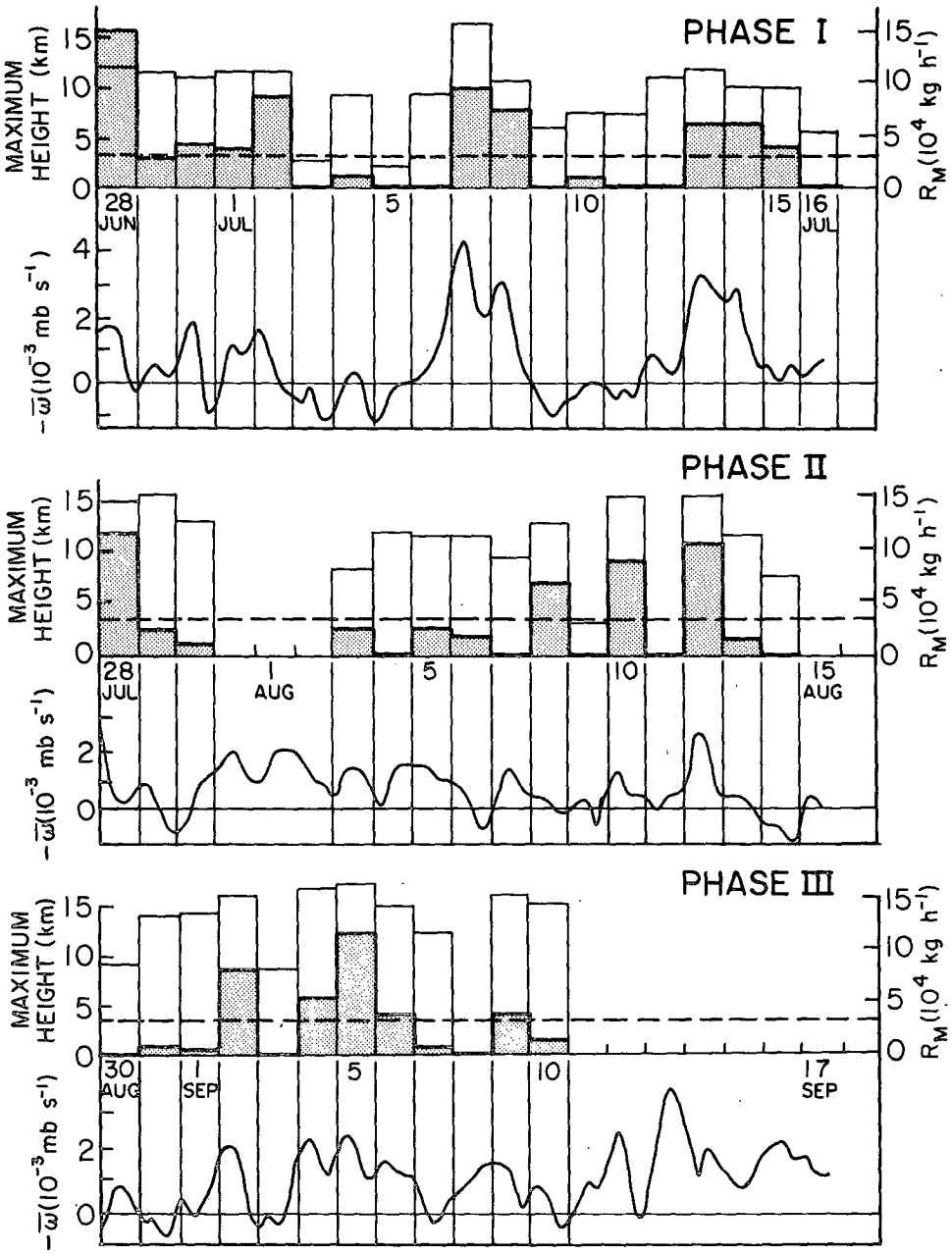

FIG. 4. Maximum echo height, mesoscale rain R_M, and mean vertical velocity $-\bar{\omega}$ for each day of GATE. Maximum echo height (unshaded histogram) and mesoscale rain (shaded histogram) are as observed with the *Oceanographer* radar. The values of $-\bar{\omega}$ are representative of the GATE B-scale array and are from Reeves *et al.* (1979). Dashed line is the threshold for marginal mesoscale rain cases mentioned in the text.

ity over the GATE B-scale ship array. The vertical velocity shown is from Reeves *et al.* (1979). Their values agree well with the computations of Thompson *et al.* (1979) for Phase III of GATE and with more recent computations for all three phases by Reed and his co-workers (personal communication). The mesoscale rainfall curve included in Fig. 4 will be discussed in Section 6.

During Phase I, overshooting was noted on only one day (7 July). The soundings for the non-overshooting days in Phase I show an average level of zero buoyancy (LZB) of ~11 km (Fig. 3a). The positive (shaded) area on this skew *T*-log*p* diagram would be cancelled by a corresponding negative area above 11 km before an undiluted parcel lifted from the surface could rise above 14 km. Conse-

TABLE 1. Days on which overshooting echoes were observed with strong and weak large-scale upward air motion. R_M is the mesoscale rainfall rate at 1200 GMT in units of 10^4 kg h^{-1} on the indicated day. The mean values of R_M for strong or weak upward motion days are also shown.

	Overshooting days with strong large-scale upward motion ($-\bar{\omega} > 0.5 \times 10^{-3}$ mb s^{-1})		Overshooting days with weak large-scale upward motion ($-\bar{\omega} < 0.5 \times 10^{-3}$ mb s^{-1})	
	Date	R_M	Date	R_M
Phase I	7 Jul	9.4	None	0
Phase II	28 Jul	11.2		
			29 Jul	2.2
	10 Aug	8.3		
	12 Aug	10.1		
Phase III			31 Aug	0.6
			1 Sep	0.5
	2 Sep	8.0		
	4 Sep	5.1		
	5 Sep	11.4		
	6 Sep	3.5		
	9 Sep	3.5		
			10 Sep	1.3
		Mean 7.8		Mean 1.1

quently, the absence of overshooting during most of Phase I can be attributed to a lack of the necessary static instability.

The sounding for the one overshooting day in Phase I (Fig. 3b) shows that the LZB, at 14 km, was abnormally high for Phase I, and that there was a large positive area below the LZB. This unusually unstable condition evidently made it possible for the overshooting to occur on this day.

Phases II and III differed from Phase I in that conditional instability sufficient to support overshooting, with a level of zero buoyancy near 14 km and a large positive area below, was characteristic of the average soundings for both overshooting and non-overshooting days (Figs. 3c–3f). Since the necessary parcel instability was always present, the occurrence of overshooting must have been determined by other conditions or forcing.

Looking first for a correlation of overshooting with large-scale forcing, we note from Fig. 4 that the maximum echo heights and, particularly, the occurrence of overshooting echoes (>14 km in height), were only weakly correlated with synoptic-scale upward motion. This result is not really surprising since, the necessary instability being present, forcing on a localized scale can trigger deep convection just as effectively as synoptic-scale forcing. This result is summarized in Table 1, where the data from Fig. 4 are stratified by dividing the days on which overshooting was observed into cases in which the large-scale upward motion ($-\bar{\omega}$, where the bar represents an average over the day) did or did not exceed 0.5×10^{-3} mb s^{-1}. Qualitative examination of the radar echo patterns for each day shows that when the synoptic-scale forcing was weak, the overshooting occurred within isolated echoes in patterns which otherwise showed only suppressed, scattered convective activity (see the case of 31 August 1974 shown in Fig. 5). When the synoptic-scale forcing was strong, the overshooting echoes were found in patterns containing heavily precipitating echoes over a large portion of the area covered by radar (see the case of 12 July 1974 shown in Fig. 6). Evidently, the large-scale forcing is important for determining the area covered by heavy rain. This result is borne out by Thompson *et al.* (1979) and Reeves *et al.* (1979) who have shown that the large-scale average lifting and total rainfall over the GATE ship array were highly correlated. However, the absence of strong large-scale forcing does not preclude the occurrence of an isolated overshooting tower.

6. Association of mesoscale rainfall with deep convection and large-scale forcing

Since a significant portion of the total GATE rainfall (~40%) has been identified as mesoscale (Fig. 2), it is important to inquire into the type of convective phenomena and the type of large-scale forcing with which this mesoscale rainfall is associated. The case studies of Houze (1977) and Leary and Houze

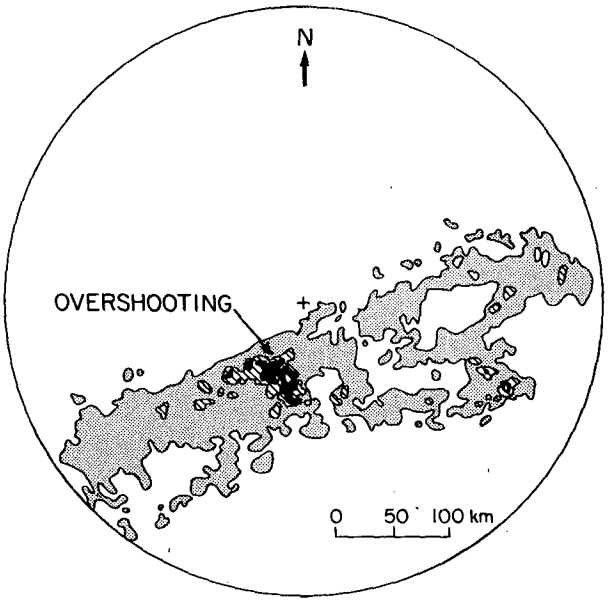

FIG. 5. *Oceanographer* radar echo pattern for 31 August 1974—a suppressed day with overshooting. Inside contours are for reflectivities of 35, 39 and 43 dBZ. Outside contour is for the minimum detectable reflectivity. Range ring is for 220 km. Plus mark shows ship position at 7.75°N, 22.2°W.

(1979a,b) have shown mesoscale rainfall to be closely associated with deep, overshooting convection. To examine whether this was more generally true, we define R_M to be the combined rate (in kilograms per second) at which water was being deposited on the sea surface by all the horizontally uniform mesoscale rain areas within the 2.8×10^5 km^{-2} area surrounding the *Oceanographer* at 1200 GMT. We have plotted the daily sequence of R_M in Fig. 4, and we have included the value of R_M for all of the overshooting days in Table 1. From the table it appears that the days on which overshooting was accompanied by strong large-scale upward motion (or forcing), the mesoscale rainfall rate was large, ranging from 3.5×10^4 to 11.4×10^4 kg h^{-1}, whereas for the days on which overshooting was accompanied by weak large-scale forcing, the values of R_M were much less, ranging from 0.5×10^4 to 2.2×10^4 kg h^{-1}. Application of Student's t-test to the values of R_M in the table leads to the conclusion that at the 1% level of significance the two columns of numbers were indeed drawn from significantly different populations. This result is consistent with our qualitative examination of the echo patterns in Section 5, which showed that the overshooting echoes on days with weaker large-scale upward motion were smaller and more isolated than on days with stronger large-scale lifting.

In Table 1, we have examined only overshooting days, that is, days with maximum echo tops over 14 km. However, Fig. 4 shows that significant amounts of mesoscale rain were observed on several days when echoes did not reach 14 km, particularly during Phase I. Table 2 lists all the days for which R_M exceeded 3×10^4 kg h^{-1}, a threshold suggested by Table 1, where this mesoscale rainfall rate was found to be exceeded on all of the overshooting days that had strong large-scale upward motion. Days on which this threshold was just barely exceeded, or, more precisely, days for which the value of R_M lay between 3 and 4.5×10^4 kg h^{-1}, are indicated as "marginal" in Table 2. That R_M only marginally exceeded the threshold on these days is clearly seen in Fig. 4. It also can be seen from the figure that the non-marginal days listed in Table 2 stand out as the really major mesoscale precipitation events in GATE.

TABLE 2. Association of significant mesoscale rainfall with large-scale upward motion and maximum convective echo height. "Marginal" refers to cases for which $R_M < 4.5 \times 10^4$ kg h^{-1}. For days when the maximum convective echo height did not exceed 14 km, the observed maxima (km) are given in parentheses.

	Days with significant mesoscale rain ($R_M > 3 \times 10^4$ kg h^{-1})	Maximum convective echo height >14 km	Large-scale upward motion $-\bar{\omega} > 0.5 \times 10^{-3}$ mb s^{-1}
Phase I	28 Jun	no (12.1)	yes
	30 Jun (marginal)	no (11.2)	no
	1 Jul (marginal)	no (11.5)	no
	2 Jul	no (11.4)	yes
	7 Jul	yes	yes
	8 Jul	no (11.2)	yes
	13 Jul	no (11.8)	yes
	14 Jul	no (10.3)	yes
	15 Jul (marginal)	no (10.0)	no
Phase II	28 Jul	yes	yes
	8 Aug	no (13.1)	no
	10 Aug	yes	yes
	12 Aug	yes	yes
Phase III	2 Sep	yes	yes
	4 Sep	yes	yes
	5 Sep	yes	yes
	6 Sep (marginal)	yes	yes
	9 Sep (marginal)	yes	yes

The maximum convective echo heights associated with the days with significant mesoscale rain (middle column, Table 2) consistently approached or exceeded the 14 km level throughout Phases II and III. The only case not actually exceeding 14 km was on 8 August, and then the maximum top was 13.1 km, probably not significantly less than 14 km. In Phase I, the maximum echo tops exceeded 14 km on only one day (7 July). On the rest of the significant mesoscale rain days in Phase I, the maximum echo tops were within ±1 km of the 11 km level, well short of 14 km. It must be remembered, however, that the level of zero buoyancy on the non-overshooting days of Phase I averaged ~11 km. It then becomes clear that all of the significant mesoscale rainfall events which

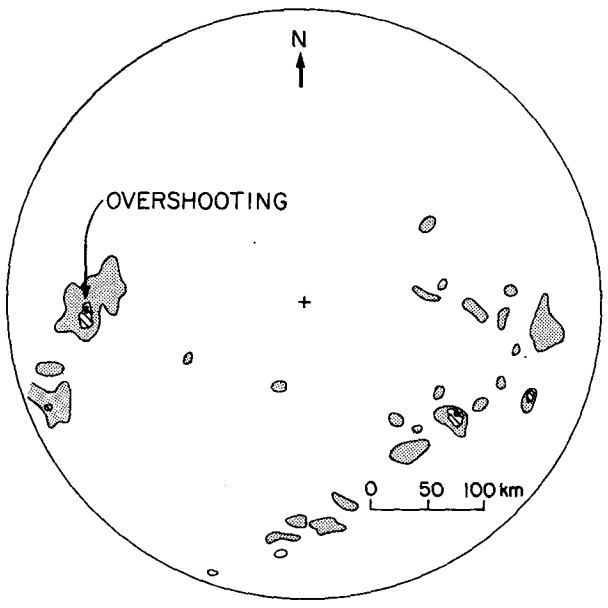

FIG. 6. *Oceanographer* radar echo pattern for 12 July 1974—an active overshooting day. Contours are for reflectivities of 35 and 39 dBZ. Outside contour is for minimum detectable reflectivity. Range ring is for 220 km. Plus mark shows ship position at 7.75°N, 22.2°W.

we sampled were associated with convective echoes having maximum tops near or above the level of zero buoyancy which prevailed during the particular phase of GATE in which they were observed.

The last column in Table 2 shows that strong large-scale motion ($-\bar{\omega} > 0.5 \times 10^{-3}$ mb s^{-1}) occurred on all but four of the days with significant mesoscale rain. However, three of these exceptional cases were days of marginal mesoscale rainfall. For the non-marginal days, there was only one case (8 August) without strong large-scale upward motion. On this day the forcing must have been subsynoptic in scale. There is no apparent reason why a significant mesoscale rain area could not be associated with subsynoptic-scale forcing. However, since there is only one strong case of this type in Table 2, we conclude that large mesoscale rainfall events are associated primarily with forcing which is synoptic in scale, more specifically, with a combination of synoptic-scale forcing and deep convection in which towers penetrate to near or above their levels of zero buoyancy. Inspection of Fig. 4 verifies, furthermore, that there were no days on which the simultaneous occurrence of strong large-scale ascent ($-\bar{\omega} > 0.5 \times 10^{-3}$ mb s^{-1}) and maximum convective echo tops at or above the level of zero buoyancy was *not* accompanied by significant mesoscale rain ($R_M > 2 \times 10^3$ kg h^{-1}).

Finally, the question arises whether synoptic or mesoscale ascent forces the mesoscale rain events directly or triggers deep convection which, in turn, develops quasi-uniform mesoscale precipitation areas. First, we note again from Table 2 that deep convection, with maximum tops approaching or exceeding the level of zero buoyancy, always accompanied significant mesoscale rain events. This observation is consistent with the development of mesoscale rain as an adjunct to deep convection. Moreover, the case studies of Houze (1977) and Leary and Houze (1979a,b) show how the uniform mesoscale rain fell from anvil clouds that had evolved from lines of deep, overshooting convection. And in Brown's (1979) numerical model, the precipitating anvil is also seen to evolve from a line of convection. These results lead us to believe that synoptic-scale, or occasionally mesoscale, ascent probably forces the heavy mesoscale precipitation events indirectly by first triggering areas of deep convection from which the mesoscale rain evolves.

7. Conclusions

The principal conclusions of this study are as follows:

1) Approximately 40% of the precipitation in GATE fell in generally horizontally uniform, slowly varying mesoscale regions of large radar echoes. This *mesoscale* rain apparently fell mostly from large anvil clouds and is significantly less intense, but covers much larger areas and is more persistent than the rain in the actively convective portions of echoes.

2) The remaining 60% of the precipitation in GATE fell in actively convective cores, either embedded in large echoes, where they co-existed with the mesoscale rain, or as isolated, small (<100 km^2) echo entities. Most of this *convective* rain fell from deep radar echoes. Very little convective rain was associated with convective echo regions with maximum tops <5 km. The amount of convective rain increased as the maximum echo heights increased from 5 km to a maximum near 12 km. A secondary maximum was produced near 15–16 km by echoes which overshot the tropopause.

3) Overshooting convective echoes were rare in Phase I of GATE, when the level of zero buoyancy for undiluted parcels tended to be near 11 km, but relatively common later in the summer, during Phases II and III, when the average level of zero buoyancy rose to 14 km.

4) When the overshooting echoes coincided with weak synoptic-scale vertical motion, they were relatively isolated and accompanied by fairly small amounts of mesoscale rain. When the overshooting echoes occurred in an environment of strong synoptic-scale upward motion, they were embedded in more widespread echoes which contained large amounts of horizontally uniform mesoscale precipitation.

5) Major occurrences of mesoscale (or anvil) rain were always accompanied by convective echoes which had maximum echo tops near the level of zero buoyancy which prevailed during the phase of GATE in which they were observed.

6) The major events of mesoscale rain in GATE tended to occur when the deep convective cells with which they were associated coincided with incidences of strong synoptic-scale upward motion.

The occurrence of large amounts of mesoscale rain in GATE points out a possible shortcoming in present approaches to diagnosing and parameterizing the properties of tropical cloud ensembles and their effects on large-scale environment. The usual practice is to assume that all of the precipitation in tropical cloud groups is associated exclusively with cumulus-scale updrafts and downdrafts. The large amounts of observed mesoscale rain suggest that mesoscale circulations associated with precipitating anvil clouds, which are larger in time and space scale than cumulus updrafts and downdrafts but still smaller than synoptic scale, may substantially affect synoptic-scale mass, heat and momentum budgets in the ITCZ. Moreover, the systematic association of significant mesoscale precipitation events with a particular combination of deep convection and strong large-scale upward

motion suggests that these events might have some degree of predictability, and, hence, it might be possible to parameterize their effects on synoptic-scale flow patterns. Future studies would be well-directed, therefore, toward determining the properties of mesoscale anvil circulations and calculating their contributions to large-scale mass and heat budgets.

Acknowledgments. We acknowledge Dr. Michael D. Hudlow for his advice in processing the *Oceanographer* radar data and Prof. Colleen A. Leary for many helpful discussions regarding the study. Prof. Richard J. Reed read the manuscript and with Mr. Ernest E. Recker provided us with GATE sounding data. Mr. Robert W. Reeves made his vertical velocity calculations available to us. This research was supported by the Global Atmospheric Research Program, Division of Atmospheric Sciences, National Science Foundation and the GATE Project Office, National Oceanic and Atmospheric Administration under Grants ATM74-14830 A01 and ATM78-16859.

REFERENCES

Austin, P. M., and S. G. Geotis, 1979: Raindrop sizes and related parameters for GATE. *J. Appl. Meteor.*, **18**, 569–575.

Battan, L. J., 1973: *Radar Observation of the Atmosphere.* The University of Chicago Press, 324 pp.

Brown, J. M., 1979: Mesoscale unsaturated downdrafts driven by rainfall evaporation: a numerical study. *J. Atmos. Sci.*, **36**, 313–338.

Cunning, J. B., and R. I. Sax, 1977: A Z–R relationship for the GATE B-scale array. *Mon. Wea. Rev.*, **105**, 1330–1336.

Gray, W. M., and R. W. Jacobson, Jr., 1977: Diurnal variation of deep cumulus convection. *Mon. Wea. Rev.*, **105**, 1171–1188.

Houze, R. A., 1977: Structure and dynamics of a tropical squall-line system. *Mon. Wea. Rev.*, **105**, 1540–1567.

——, and C. A. Leary, 1976: Comparison of convective mass and heat transport in tropical easterly waves computed by two methods. *J. Atmos. Sci.*, **33**, 424–429.

——, and C.-P. Cheng, 1977: Radar characteristics of tropical convection observed during GATE: Mean properties and trends over the summer season. *Mon. Wea. Rev.*, **105**, 964–980.

Hudlow, M. D., 1975: Oceanographer radar images on 16 mm microfilm. *GATE Processed and Validated Data*, GATE World DATA Center A, National Climatic Center, NOAA, Federal Bldg., Asheville, NC, 50 pp.

——, 1976: Documentation for GATE NOAA radar hybrid data. *GATE Processed and Validated Data*, GATE World Data Center A, National Climatic Center, NOAA, Federal Bldg., Asheville, NC, 31 pp.

——, 1978: Hourly radar precipitation PPI graphics. *GATE Processed and Validated Data*, GATE World Data Center A, National Climatic Center, NOAA, Federal Bldg., Asheville, NC, 13 pp.

——, R. Arkell, V. Patterson, P. Pytlowany, F. Richards and S. G. Geotis, 1978: Calibration and intercomparison of the GATE C-band radars. NOAA Tech. Rep. EDS 31, Center for Environmental Assessment Services, NOAA, Washington (in press).

Johnson, R. H., 1976: The role of convective-scale precipitation downdrafts in cumulus and synoptic-scale interactions. *J. Atmos. Sci.*, **33**, 1890–1910.

Leary, C. A., and R. A. Houze, Jr., 1979a: The structure and evolution of convection in a tropical cloud cluster. *J. Atmos. Sci.*, **36**, 437–457.

——, and R. A. Houze, Jr., 1979b: Melting and evaporation of hydrometeors in precipitation from the anvil clouds of deep tropical convection. *J. Atmos. Sci.*, **36**, 670–679.

López, R. E., 1973: Cumulus convection and larger scale circulation, II. Cumulus and mesoscale interaction. *Mon. Wea. Rev.*, **101**, 856–870.

——, 1976: Radar characteristics of the cloud populations of tropical disturbances in the northwest Atlantic. *Mon. Wea. Rev.*, **104**, 269–283.

——, 1978: Internal structure and development processes of C-scale aggregates of cumulus clouds. *Mon. Wea. Rev.*, **106**, 1488–1494.

Malkus, J. S., and H. Riehl, 1964: *Cloud Structure over the Tropical Pacific Ocean.* University of California Press, 229 pp.

McGarry, M. M., and R. J. Reed, 1978: Diurnal variations in convective activity and precipitation during Phases II and III of GATE. *Mon. Wea. Rev.*, **106**, 101–113.

Ogura, Y., and H.-R. Cho, 1973: Diagnostic determination of cumulus cloud populations from observed large-scale variables. *J. Atmos. Sci.*, **30**, 1276–1286.

——, and Y.-L. Chen, 1977: A life history of an intense mesoscale convective storm in Oklahoma. *J. Atmos. Sci.*, **34**, 1458–1476.

Plank, V. E., 1969: The size distributions of cumulus clouds in representative Florida populations. *J. Appl. Meteor.*, **8**, 46–67.

Reeves, R. W., C. F. Ropelewski and M. D. Hudlow, 1979: On the relationship of the precipitation to variations in the kinematic variables during GATE. *Mon. Wea. Rev.*, **107**, 1154–1168.

Riehl, H., and J. S. Malkus, 1958: On the heat balance of the equatorial trough zone. *Geophysica*, **6**, 503–538.

Sanders, F., and R. J. Paine, 1975: The structure and thermodynamics of an intense mesoscale convective storm in Oklahoma. *J. Atmos. Sci.*, **32**, 1563–1579.

——, and K. A. Emanuel, 1977: The momentum budget and temporal evolution of a mesoscale budget and temporal evolution of a mesoscale convective system. *J. Atmos. Sci.*, **34**, 322–330.

Thompson, R. M., Jr., S. W. Payne, E. E. Recker and R. J. Reed, 1979: Structure and properties of synoptic-scale wave disturbances in the Intertropical Convergence Zone of the eastern Atlantic. *J. Atmos. Sci.*, **36**, 53–72.

Yanai, M., S. Esbensen and J.-H. Chu, 1973: Determination of the bulk properties of tropical cloud clusters from large-scale heat and moisture budgets. *J. Atmos. Sci.*, **30**, 611–627.

Zipser, E. J., 1969: The role of organized unsaturated convective downdrafts in the structure and decay of an equatorial disturbance. *J. Appl. Meteor.*, **8**, 799–814.

——, 1977: Mesoscale and convective-scale downdrafts as distinct components of squall-line circulation. *Mon. Wea. Rev.*, **105**, 1568–1589.